Journal of *Marine Science and Engineering*

MDPI

Article

Wave Energy Resource Assessment for Small-Scale WEC near a Harbour

Nicolas Guillou *, Georges Chapalain and Philippe Sergent

Cerema, DtecREM, HA, 155 rue Pierre Bouguer, Technopôle Brest-Iroise, BP 5, 29280 Plouzané, France
* Correspondence: nicolas.guillou@cerema.fr; Tel.: +33-29805-6739

Abstract: Accurate evaluations of the available and technically exploitable wave energy resources are fundamental to optimise the design and implementation of energy converters in the marine environment. However, long-term resource assessments have been primarily conducted for large-scale devices in offshore energetic locations, thus ignoring onshore sites such as harbours with easier access, installation and accessibility to devices. Here, we conducted a ten-year evaluation of the performance of wave energy converters (WECs) off Roscoff harbour (northern Brittany, France). As the site of application shows moderately energetic conditions, particular attention was dedicated to small-scale WECs by adapting ratings to the local wave climate. This investigation combined (i) a high-spatial resolution (~5 m) hindcast database established with SWAN with (ii) generic and specific assessments of WEC performance. We exploited, in particular, scaled power matrices derived from the Oyster technology to assess the capacity factors and energy output of devices. In addition to characterising the annual and seasonal variability of the available resource off the harbour breakwater, this investigation provided further insights for optimising WECs, including experimental prototypes. It is therefore suggested that this type of evaluation be considered for the assessment of small- and/or full-scale energy converters in the marine environment.

Keywords: wave energy converters; wave climate; hindcast database; SWAN; temporal variability; capacity factor; power matrix; Roscoff; western Brittany

check for updates

Citation: Guillou, N.; Chapalain, G.; Sergent, P. Wave Energy Resource Assessment for Small-Scale WEC near a Harbour. *J. Mar. Sci. Eng.* **2022**, *10*, 1081. https://doi.org/10.3390/jmse10081081

Academic Editor: Diego Vicinanza

Received: 24 June 2022
Accepted: 26 July 2022
Published: 7 August 2022

1. Introduction

Nearshore areas may present an increased attractiveness for wave energy exploitation, thus providing easier access, installation and accessibility of wave energy converters (WECs) with reduced operation and maintenance costs. Over the last few years, much interest has thus been brought to the development of WECs adapted to or embedded within coastal infrastructures such as harbour dikes or breakwaters. A detailed review of these different systems is available in [1,2]. Among the leading projects, we may refer to the oscillating float devices developed by (i) Ingine, with a prototype tested in Buckdon Harbour (Jeju-do Island, Korea), [3] or (ii) Eco Wave Power with an array of eight energy converters implemented in Gibraltar and connected to the grid [4]. Other devices include (i) overtopping systems, such as the Overtopping Breakwater for Wave Energy Conversion (OBREC) with a full-scale prototype implemented at Naples Harbour (Italy) [5,6], or (ii) oscillating water columns (OWC), such as the Resonant Wave Energy Converter 3 (REWEC3) with a device operating in the Port of Civitavecchia (Italy) [7] or the Wavegen system implemented in the power plant of Mutriku Harbour (Spain) [8].

However, in spite of these advanced technical developments, wave energy conversion still shows high economic uncertainty mainly associated with performance, lifespan, construction and maintenance costs of WECs, which has until now impacted an increased exploitation at commercial scale [9]. Among the key steps for promoting the growth of the wave energy sector, refined assessments of the available resource and expected generated power are fundamental to optimise the location, design and construction costs of devices.

Numerical simulations are traditionally used to conduct these resource assessments. Nevertheless, these investigations have to satisfy specific constraints associated with (i) the temporal variations of the wave climate and (ii) the spatial extent of the area of interest. Thus, according to the technical specification set up by the Marine Renewable Energy Technical Committee (TC114) of the International Electrotechnical Commission (IEC) [10], resource assessments should cover a minimum period of ten years to encompass the interannual and interseasonal variability of the wave energy flux. Additionally, longer time periods extending to 20, 30 or even 100 years may be requested for more accurate characterisation of the wave energy resource, including the approach of (i) the return periods of wave events [11,12] or (ii) the effects of global warming on the wave climate [13,14]. Furthermore, increased spatial resolutions are expected in harbour areas where the computational mesh must adapt to the outline of infrastructure and the spatial variability of surrounding water depths, which decrease to a few metres.

Given the large computational resource required, few numerical investigations were therefore conducted to assess wave climate variability in the vicinity of harbour areas, matching constraints of an extended period of time (at least 10 years) and increased spatial resolutions (on the order of metres). Thus, wave energy resource assessments near harbours have relied on hindcast simulations with phase-averaged models and spatial resolutions reaching values over one hundred metres, thus poorly adapted to the dimensions of maritime structures. Contestabile et al. [5] characterised the potential of the OBREC in different harbours of southwestern Australia by relying on MIKE 21 SW simulations with spatial resolutions of 150 m. More recently, Lastiri et al. [15] built a 44-year wave hindcast database with SWAN (Simulating Wave Nearshore) [16] to assess energy spatiotemporal variability in the surroundings of Bayonne Harbour (Bay of Biscay, France) with a minimum onshore spatial resolution of 150 m. Another investigation was conducted by Cascajo et al. [17] in the surroundings of the Port of Valencia (Spain) by exploiting WAM large-scale embedded simulations of the wave climate over a seven-year period.

The present investigation complements these different characterisations of the available wave energy resource in harbour areas with an advanced evaluation based on (i) embedded high-resolution numerical simulations of the wave climate and (ii) refined assessments of WEC performance. Thus, meeting the IEC standards, we established a ten-year wave hindcast database in the vicinity of the harbour breakwater with the SWAN wave model set up at a spatial resolution of 5 m. As exhibited before, more accurate resource characterisations may be reached by extending the period of simulations to 20–30 years. However, given the refined spatial resolutions reached near the breakwater, this investigation is a step forward in conducting long-term simulations of the wave climate with higher computational resources in harbour areas. This hindcast database was therefore exploited to characterise the annual and seasonal variability of the available resource in the vicinity of the harbour. As technological characteristics of WECs were mainly available for offshore systems designed for energetic locations, device performances were first investigated with an original approach combining a generic evaluation independent from the technology. This generic assessment was then complemented by a specific evaluation based on scaled power matrices adapted to the local wave climate and derived from the Oyster technology [18,19].

The site of application is the harbour of Roscoff–Bloscon in the northern part of western Brittany (France) (Figure 1). This harbour, which welcomes fishing, yachting and freight transport activities, is the most important in France for maritime traffic to Ireland, hosting a ferry terminal for Brittany and Irish Ferries. In spite of reduced exposure to incoming waves from the Atlantic Ocean, this location is regularly subjected to local wind-generated waves from the English Channel, which may increase the wave energy resource. Thus, further investigation is required concerning the potential of this harbour for wave energy conversion. Beyond site-specific results, the present investigation also provides further insights on the potential of phase-averaged spectral wave models to assess resource temporal variability in the vicinity of harbours. The approach considered may

finally serve as a guideline to conduct a refined assessment of the available resource and expected energy output in the preliminary stages of a wave energy project.

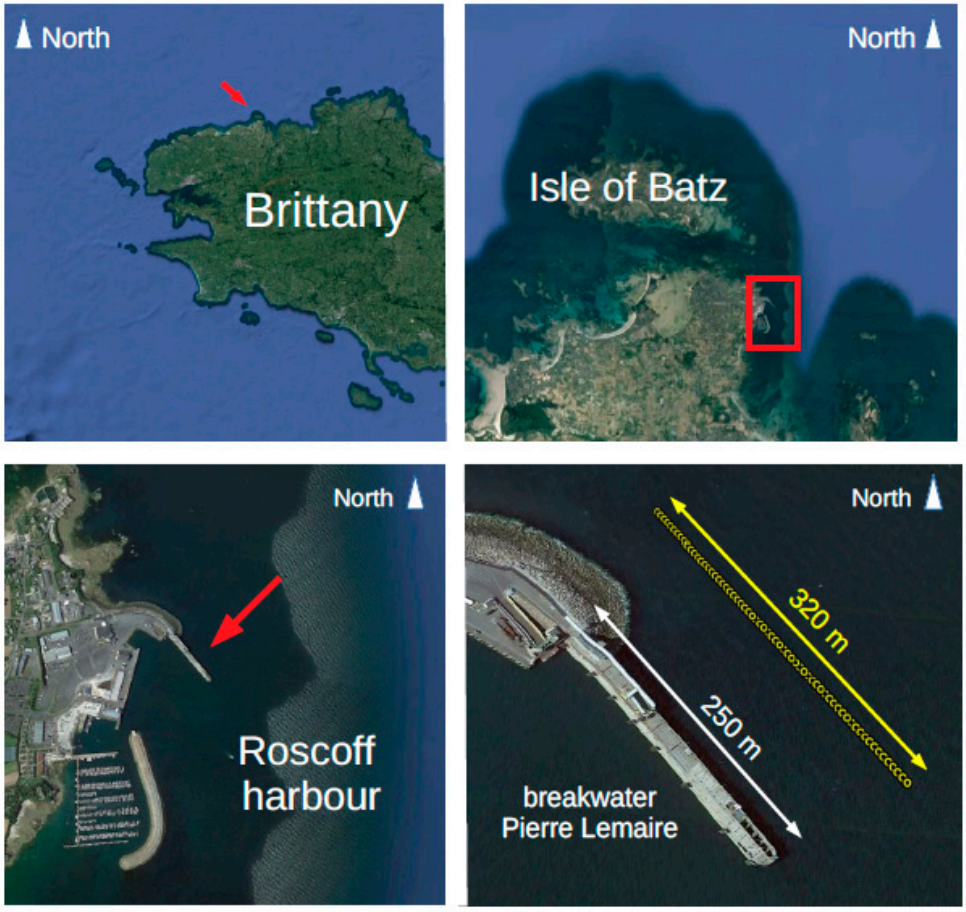

Figure 1. Google Earth maps showing the location of the harbour of Roscoff in western Brittany (France) with a detailed view of the surroundings of the breakwater "Pierre Lemaire". The yellow circles are displayed along a line considered offshore from this infrastructure; the line is used as reference for the extraction of SWAN hindcast predictions.

The present paper is organised as follows. Section 2 describes the study site including its environmental and physical characteristics. Section 3 successively presents the wave model, the available in situ measurements exploited to assess predictions, performance indicators, and wave energy metrics retained to evaluate the model performance and the temporal variability of the available resource. After a comparison between model predictions and in situ measurements (Section 4.1), Section 4.2 discusses the spatiotemporal variability of the available resource off the harbour breakwater based on exploitation of the ten-year hindcast database derived from SWAN simulations. Finally, Section 4.3 describes the generic and specific assessments of WEC performance. Beyond the comparison of indicators such as the capacity factor, particular attention is dedicated to the annual and seasonal variability in the performance of small-scale devices.

2. Study Site

The harbour of Roscoff–Bloscon is located in the northern part of western Brittany (France) between the Isle of Batz and the Bay of Morlaix (Figures 1 and 2). It integrates a Jarlan-type breakwater, entitled "Pierre Lemaire", with a length of 250 m and composed of four boxes orientated in a northwest–southeast direction. Nearshore waters are characterised by (i) numerous shoals, emerged rocks and rocky shelves, and (ii) wide wetting–drying areas revealed at low tide in the channel separating the Isle of Batz from the

landmass. The area also shows strong tidal regimes with spring tidal range over 7 m and spring tidal currents exceeding 1 m s^{-1} in the channel of Batz [20]. However, the vicinity of the breakwater rests within a minimum water depth of 7 m, thus securing the operation of energy converters.

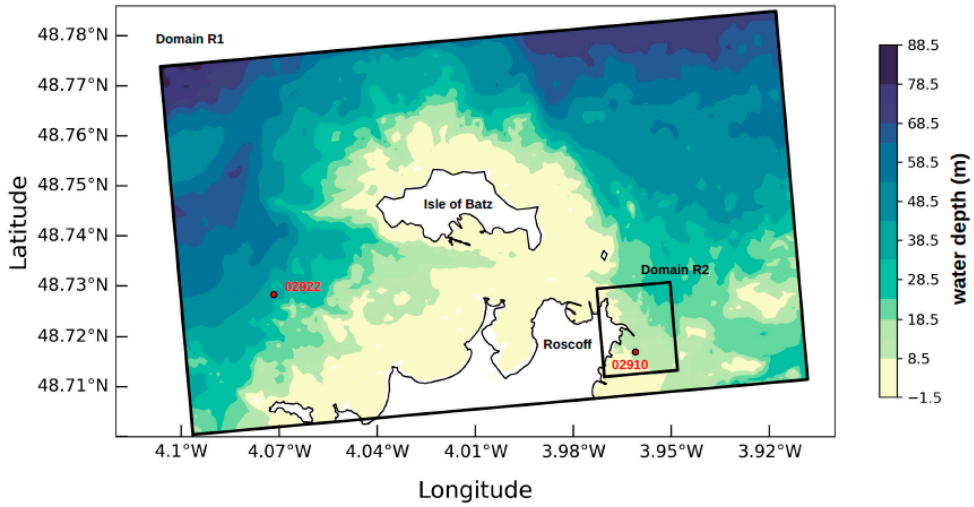

Figure 2. Spatial extent of the embedded computational domains R1 and R2 with locations of wave buoys 02922 and 02910 (CANDHIS database).

In spite of the shelter provided by the isle of Batz, the breakwater is exposed to northwesterly and northeasterly waves. Thus, the harbour is subjected to a twin exposure to (i) swell from the Atlantic Ocean refracted around the isle and (ii) wind waves generated locally in the English Channel. The analysis of measurements at the wave buoy south of the harbour (wave buoy 02910 of the French CANDHIS database, "Centre d'Archivage National de Données de Houle In Situ", Cerema, France) exhibited two prominent sea states characterised by peak periods between (i) 3 and 6 s and (ii) 8 and 14 s (Figure 3). The variability in harbour wave exposure is also increased by tide-induced refraction. Thus, tidal currents induced refraction of the waves, leading to changes of the wave direction towards areas with lower propagation speed of the crest, and this results in modulations of wave exposure with semidiurnal variations of the significant wave height and wave direction [21]. These modulations were revealed by observations gathered south of the harbour with variations of the significant wave height between high and low tides of around 30% of the same order of effects exhibited in offshore waters of western Brittany [22] (Figure 4). Increased effects were expected on the wave energy flux as a function of the squared significant wave height.

Given these physical and environmental characteristics, a refined numerical simulation of wave condition in the vicinity of the breakwater must therefore consider (i) the detailed spatial variation of surrounding water depth, (ii) the variability in incoming sea states between swell and local wind-generated waves, and (iii) the effects of the tide on coastal wave propagation (including especially the refraction induced by tidal currents).

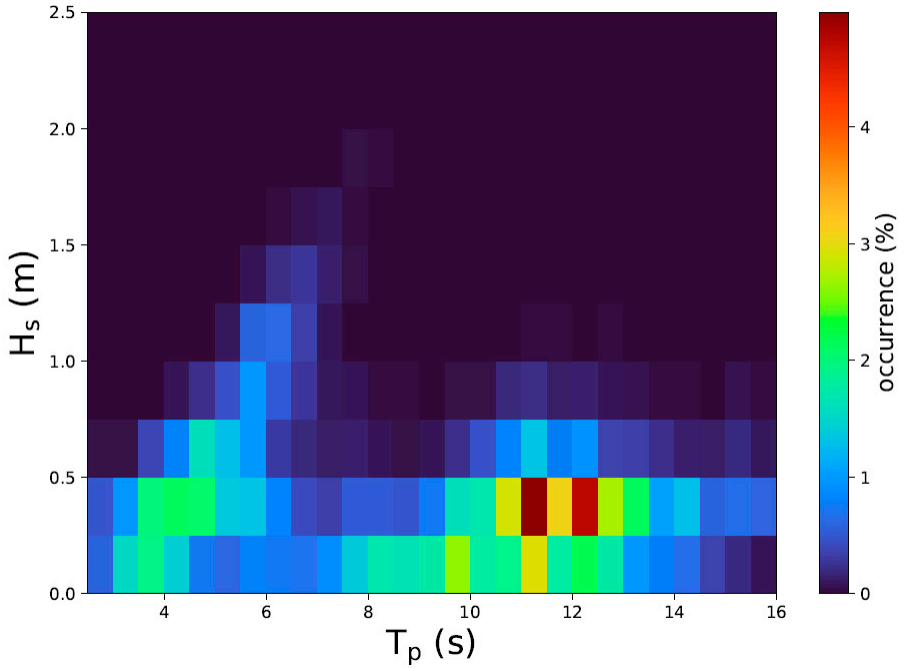

Figure 3. Mean distribution of wave events for a range of significant wave heights H_s and peak periods T_p at wave buoy 02910 during the year 2011. The color bar shows the occurrence of wave events in percentages.

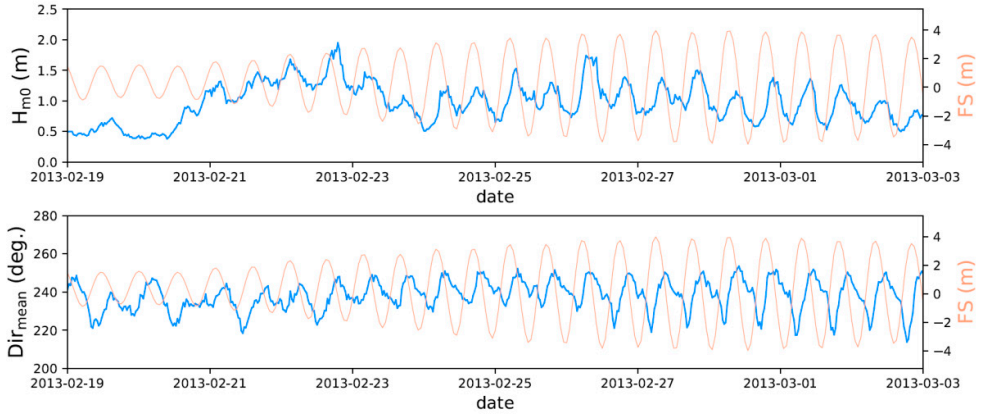

Figure 4. Time series of measured significant wave height (H_{m0}, blue line) and mean wave direction (Dir_{mean}, blue line, anticlockwise convention from east) at wave buoy 02910 and free-surface elevation (FS with respect to mean water depth, red line) at the tidal gauge in the harbour of Roscoff–Bloscon during February and March 2013.

3. Materials and Methods

3.1. Model Theoretical Description

SWAN solves the time-dependent spectral action balance equation that expresses the conservation of the wave-action density in spatial, spectral and directional spaces according to a series of source and sink terms involved in generation, dissipation and redistribution of wave energy [23]. The latest version, 41.31, of the wave model was considered here. Parametrisations retained for source and sink terms are briefly detailed hereafter. The transfer of energy from wind to waves and its dissipation due to whitecapping were approached with the model proposed by Rogers et al. [24]. The redistribution of energy by nonlinear quadruplet wave–wave interactions was computed with the discrete interaction approximation [25]. In coastal and nearshore areas, wave propagation is subjected to an increased

influence of bottom friction, nonlinear triad redistribution of wave energy and depth-induced breaking. The sink term of energy dissipation by bottom friction was computed with the coefficient retained by Bouws and Komen [26]. The nonlinear triad redistribution of wave energy was approached with the lumped triad approximation [27]. Energy dissipation in random waves due to depth-induced breaking was finally quantified according to Battjes and Janssen [28]. Further details about SWAN mathematical formulations and numerical resolution are available in the scientific and technical documentation [29].

3.2. Model Setup

SWAN was set up on two embedded computational domains: (i) a large-scale domain R1 integrating the Isle of Batz and extending to deep water, over 70 m, at the southwestern entrance of the English Channel, and (ii) a local domain R2 covering the surroundings of the harbour of Roscoff–Bloscon (Figure 2). Simulations in domain R1 were implemented to approach wave transformation from deep waters of the English Channel to the coastline, integrating large-scale refraction induced by a varying bathymetry and tidal currents (particularly noticeable around the Isle of Batz) with superimposed effects of local wind waves. Embedded simulations in domain R2 were implemented to approach the local distribution of wave energy associated with a refined definition of the bathymetry in the vicinity of the harbour breakwater. Spatial resolutions were therefore set to 100 and 5 m on domains R1 and R2, respectively. In comparison to large-scale simulations conducted in R1, simulations in R2 neglected processes with reduced effects in nearshore waters, including wave growth by wind, energy dissipation by whitecapping and nonlinear quadruplet wave–wave interactions. According to the prominent effect of the tide in wave propagation (Section 2, Figure 4), the effects of tidal free-surface elevation and depth-averaged currents were integrated. However, the effects of tidal currents were ignored in R2 to reduce the computational time. Preliminary simulations showed that this had very little impact on SWAN predictions as modulations induced by currents on waves derived, in this small-scale domain, from input forcings at open boundaries. By doing so, we neglected the local modulations induced by tidal currents in the surroundings of the harbour breakwater on the group velocity, thus considering that major effects on the available wave power derived from modulations on the wave-action density and the significant wave height. Simulations in R2 considered, however, the spatiotemporal variations of tide-induced free-surface elevations. In these two computational domains, R1 and R2, SWAN was run with a discretisation of the wave energy spectrum in 31 exponentially spaced frequencies ranging from 0.05 to 1 Hz and 30 evenly spaced directions. In R1, the model was run in nonstationary mode with a time step of 10 min. In R2, taking into account the reduced extent of this computational domain, we implemented a series of stationary computations with a step of one hour.

The spatial distribution of the bathymetry was derived from a compilation of (i) the large-scale Homonim database covering the English Channel with a spatial resolution of 0.01° (~100 m) [30] and (ii) the high-resolution coverage established during the Litto3D project with a spatial resolution up to several metres in nearshore areas [31]. In domain R1, the model was driven by Pierson–Moskowitz spectra [32] recomposed from wave components (significant wave height, peak period, direction and spreading) extracted at an hourly time step from the hindcast database Homere [33]. The Homere database consists in hindcast simulations conducted with Wavewatch III during the period 1994–2019 in French coastal shelf seas of the Atlantic Ocean and the English Channel. Wind velocity components at 10 m above the free surface were provided at a time step of one hour from spatial interpolation of Homere data. Tidal free-surface elevation and depth-averaged currents were extracted from hourly predictions conducted with a spatial resolution of 250 m as part of the MARC project [34]. In domain R2, input forcings were derived from predictions established in domain R1.

TheS extraction of input boundary conditions from the Homere database was restricted to a ten-year period between 2006 and 2015 to match IEC standards for assessment of the

wave climate and associated energy resource. Thus, simulations in domains R1 and R2 were conducted for this ten-year period.

3.3. In Situ Measurements

Available data used to assess wave model performance consist of archived wave buoy measurements from the French CANDHIS database ("Centre d'Archivage National de Données de Houle In Situ", Cerema, France). These data include (i) a location in the southwestern part of the Isle of Batz at water depths of 30 m (02922, lon = −4.072° W, lat = 48.728° N) and (ii) a location in nearshore waters south of the breakwater of Roscoff–Bloscon harbour at water depths of 5 m (02910, lon = −3.961° W, lat = 48.717° N) (Figure 2). The two wave buoys were directional, thus giving access to the direction of incoming waves. In offshore waters, data were available from 27 March 2019 to 31 December 2021, covering a period exceeding 2.5 years. In nearshore waters, measurements covered an extended period of 9.5 years from 21 October 2005 to 1 March 2015. No specific period with missing data was noticed in offshore waters, whereas blank periods were present for nearshore waters in February 2009, April and May 2010, June 2012 and August 2014. However, the measurement periods were considered sufficient to encompass the annual and seasonal variability of the wave climate. Thus, the ten-year period considered to run simulations, from 2006 to 2015, matched available in situ measurements in nearshore waters.

3.4. Performance Indicators and Wave Energy Metrics

Predictions were interpolated at the different time steps of available measurements. Performances of SWAN were evaluated by relying on a series of statistical and scoring metrics. For the significant wave height and the wave period, we considered (i) the mean absolute error

$$MAE = \sum_{i=1}^{N} \mid S_i - O_i \mid \Big/ N \tag{1}$$

(ii) the normalised bias

$$NBI = \sum_{i=1}^{N} (S_i - O_i) \Big/ \sum_{i=1}^{N} O_i \tag{2}$$

and (iii) the symmetrically normalised root mean square error introduced by Hanna and Heinold [35]

$$HH = \sqrt{\sum_{i=1}^{N} (S_i - O_i)^2 \Big/ \sum_{i=1}^{N} S_i O_i} \tag{3}$$

with N the number of data in the discretised times series considered, and (S_i) and (O_i) the two sets of simulated and observed values, respectively. For the wave direction, following Kalourazi et al. [36], we relied on the modified normalised bias

$$NBI_\theta = \sum_{i=1}^{N} mod_{-\pi,\pi}(\theta_{Si} - \theta_{Oi}) / (2\pi N) \tag{4}$$

and the normalised root mean square error

$$NRMSE_\theta = 1/(2\pi) \sqrt{\sum_{i=1}^{N} [mod_{-\pi,\pi}(\theta_{Si} - \theta_{Oi})]^2 \Big/ N} \tag{5}$$

Module operator $mod_{-\pi,\pi}$ indicates that (i) 2π is subtracted from $\theta_{Si} - \theta_{Oi}$ if $\theta_{Si} - \theta_{Oi} > \pi$ and (ii) 2π is added to $\theta_{Si} - \theta_{Oi}$ if $\theta_{Si} - \theta_{Oi} < -\pi$. As exhibited by Mentaschi et al. [37], traditional indicators such as the root mean squared error (RMSE) or the scatter index (SI) may show biases to identify the best performance associated with wave numerical models.

Thus, other indicators including the HH are currently exploited to assess model accuracy. The NBI index complements the MAE by providing further information about the average component of the error. The HH index combines information about the average component of the error and the scatter component.

Pre-production metrics were also considered to characterise the temporal variability of the resource at different time scales (ranging from annual to monthly) (see [9] for a review). In the present investigation, we focused on the intra-annual and monthly differentiations in the resource. Thus, following [38,39], we considered the annual variability index

$$AVI = (P_{A1} - P_{A2})/P_{year} \quad (6)$$

with P_{year} the annual mean wave power, and P_{A1} and P_{A2} the mean available wave powers for the most and the least energetic years, respectively. As the seasonal variability was mainly affected by differences in the resource between months, we retained the monthly variability index

$$MVI = (P_{M1} - P_{M2})/P_{year} \quad (7)$$

with P_{M1} and P_{M2} the mean powers for the most and the least energetic months, respectively.

4. Results and Discussion

4.1. Evaluation of Model Predictions

Model performances in domain R1 were assessed against measurements in offshore waters (southwestern part of the Isle of Batz (wave buoy 02922)) whereas performances in domain R2 were evaluated against measurements in nearshore waters (south of the breakwater (wave buoy 02910)). The comparison focused on the significant wave height H_{m0}, the peak period T_p and the mean wave direction Dir_{mean}.

In domain R1, the comparison was conducted for the year 2019 between 27 March 2019 and 31 December 2019 in accordance with the availability of measurements for this period. Predictions approached the temporal evolution of parameters measured at wave buoy 02922 (Figure 5). A clear contrast was exhibited between (i) the winter period characterised by increased variability in energetic conditions and (ii) the summer period with reduced variability of wave events. These differences were particularly noticeable between the two periods July–September and October–December. Such contrasting conditions were consistent with assessments conducted in western Brittany, which exhibited the strong interseasonal and interannual evolutions of the available resource [40,41]. In northwest continental shelf seas, this variability is highly dependent on oscillations of the atmospheric circulation resulting in increased correlations between significant wave heights and the North Atlantic Oscillation (NAO) [42]. Furthermore, performance indicators for the evaluation of H_{m0} and T_p were consistent with estimations derived from spectral phase-averaged wave models in coastal waters with HH indexes below 0.2 [36,43] (Table 1). SWAN showed, however, a tendency to underestimate high sea state characterised by $H_{m0} > 4$ m (Figure 5). For reduced energetic conditions, the model was also found to slightly overestimate the measured significant wave height, as confirmed by the associated positive NBI (Table 1). However, these differences were very small, and these comparisons assessed a part of the wave model performance to approach wave conditions in the large-scale domain R1.

In domain R2, the comparison covered the period between 2006 and 2015. SWAN reproduced the temporal evolutions of H_{m0}, T_p and Dir_{mean} measured in the southern part of the harbour breakwater at wave buoy 02910 (Figure 6). Whereas the model ignored the spatiotemporal variations of tidal currents, predictions approached the tide-induced modulations of significant wave height and wave direction. This confirmed that these modulations resulted from input forcings at open boundaries of domain R2. Statistical scorings showed, however, stronger differences than those obtained in offshore waters at wave buoy 02922. This concerned especially H_{m0} and T_p with HH values over 0.3 (Table 1). We also obtained an increased NBI for the peak period with values of 0.27 in nearshore waters against 0.04 in offshore waters. Nevertheless, scorings remained consistent with

performance of phase-averaged wave models. Thus, Mentaschi et al. [43] found HH indexes between 0.28 and 0.32 for the approach of the significant wave height in a series of wave buoys located in coastal waters of the Mediterranean Sea. In the present investigation, we obtained an HH value of 0.32 for the approach of H_{m0} during the period from 2006 to 2015, this in spite of strong tide-induced modulations and a potential influence of diffraction induced by the harbour breakwater and not considered by the phase-averaged spectral wave model. Thus, whereas increased differences were obtained in nearshore waters, no particular bias was denoted, and the comparisons confirmed the capability of the SWAN model to approach wave propagation at the scale of domain R2.

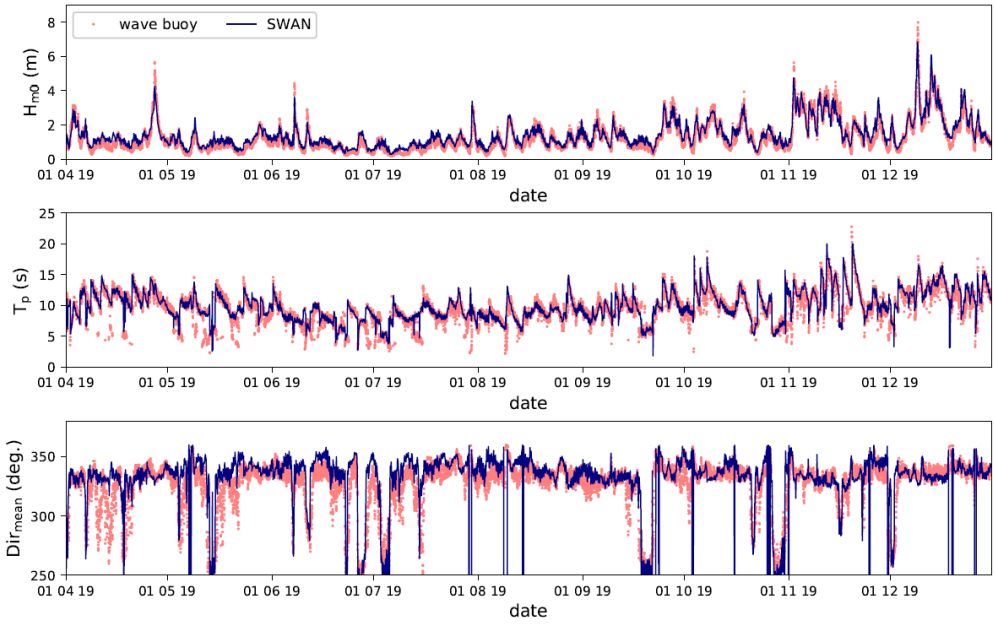

Figure 5. Times series of measured and computed significant wave height H_{m0}, peak period T_p and mean wave direction Dir_{mean} (anticlockwise convention from east) between April and December 2019 at wave buoy 02922 in the western part of domain R1.

Table 1. Statistics for the evaluation of the significant wave height H_{m0}, peak period T_p and mean wave direction Dir_{mean} at the two wave buoys considered. Statistics at wave buoy 02922 were computed for the year 2019 (from end of March to the end of the year) whereas statistics at wave buoy 02910 were computed from 1 January 2006 to 1 March 2015 in relation to the availability of in situ measurements at these two locations. Further details about the mathematical formulations of these metrics are available in Section 3.4. Please also note that, with an exception for the mean absolute error (MAE), these metrics correspond to normalised parameters.

Wave Buoys	H_{m0}			T_p			Dir_{mean}	
	MAE	NBI	HH	MAE	NBI	HH	NBI_θ	$NRMSE_\theta$
02922	0.25 m	0.12	0.19	0.99 s	0.04	0.16	0.018	0.05
02910	0.13 m	0.13	0.32	2.70 s	0.27	0.40	0.0004	0.05

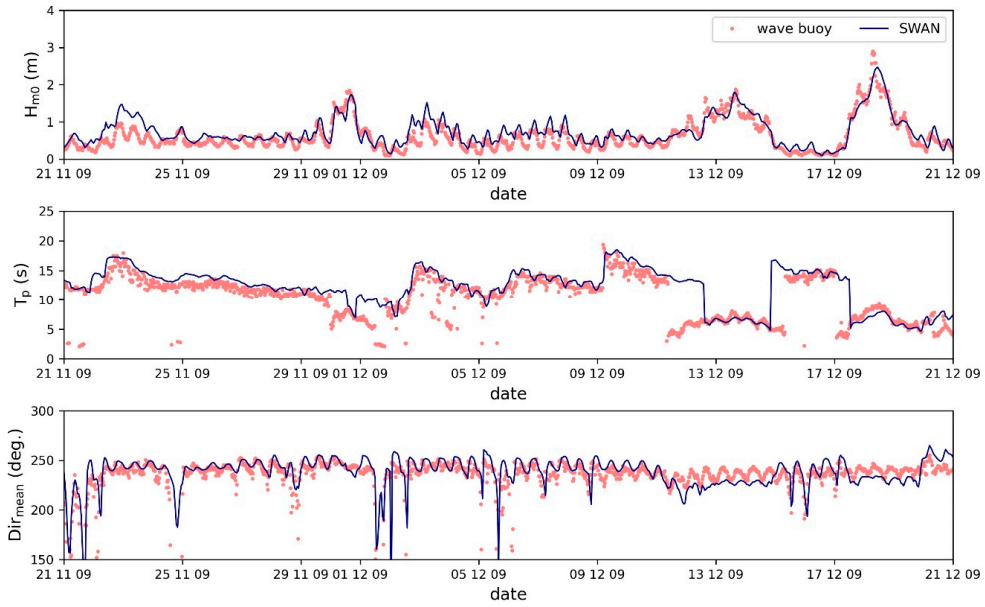

Figure 6. Time series of measured and computed significant wave height H_{m0}, peak period T_p and mean wave direction Dir_{mean} (anticlockwise convention from east) at wave buoy 02910.

4.2. Spatiotemporal Variability of Available Wave Energy

Particular interest was devoted to the spatial and temporal variability of the available wave energy resource in the vicinity of the harbour. Thus, wave predictions were analysed along a line offset at a distance of 100 m from the breakwater. Moving away the implementation of WEC from the infrastructure maintains access to the breakwater, including especially the Brittany and Irish Ferries. This distance was restricted to 100 m, however, to guarantee cable connection, and device operation and maintenance. As the breakwater was made of perforated caissons of Jarlan-type, designed to reduced reflection effects (Section 2), weaker influence of the breakwater was finally expected on sea state conditions at this distance of 100 m. Along this line, we extracted predictions from SWAN in subdomain R2 (i) at a time step of one hour during the ten-year period (from 2006 to 2015) and (ii) a spatial resolution of 5 m. Thus, this line had a length of 320 m extending from a northwestern point off the rockfill section at the foot of the breakwater to a southeastern point near the entrance of the harbour (Figure 1). The attention was first dedicated to the spatial distribution of averaged wave parameters (including significant wave height and available wave power) before focusing on resource temporal variability.

Figure 7 shows the spatial distribution of the averaged and maximum significant wave height and available wave energy flux along this line, which lies off the harbour breakwater. The vicinity of the harbour was characterised by moderate wave regimes with averaged H_{m0} between 0.5 and 0.6 m. However, the harbour may also be exposed to storm sea wave conditions with significant wave heights exceeding 3.5 m. Furthermore, the surroundings of the harbour were characterised by a spatial gradient in the distribution of H_{m0}, which revealed an increased exposure of the northwestern area off the rockfill section at the foot of the breakwater (Figures 1 and 7). These differences were exhibited by the spatial distribution of the available wave energy flux. Whereas the mean wave power was very low with values below 2 kW m^{-1}, storm events showed a more important potential exceeding 60 kW m^{-1}, the same order of averaged values found in offshore waters of western Brittany [41]. Furthermore, the spatial gradient in maximum available wave power exhibited differences of around 15 kW m^{-1} between the northwestern and southeastern ends of the line considered offshore from the harbour infrastructure. These results promote the exploitation of the wave resource in the northwestern area identified off the rockfill section at the foot of the breakwater.

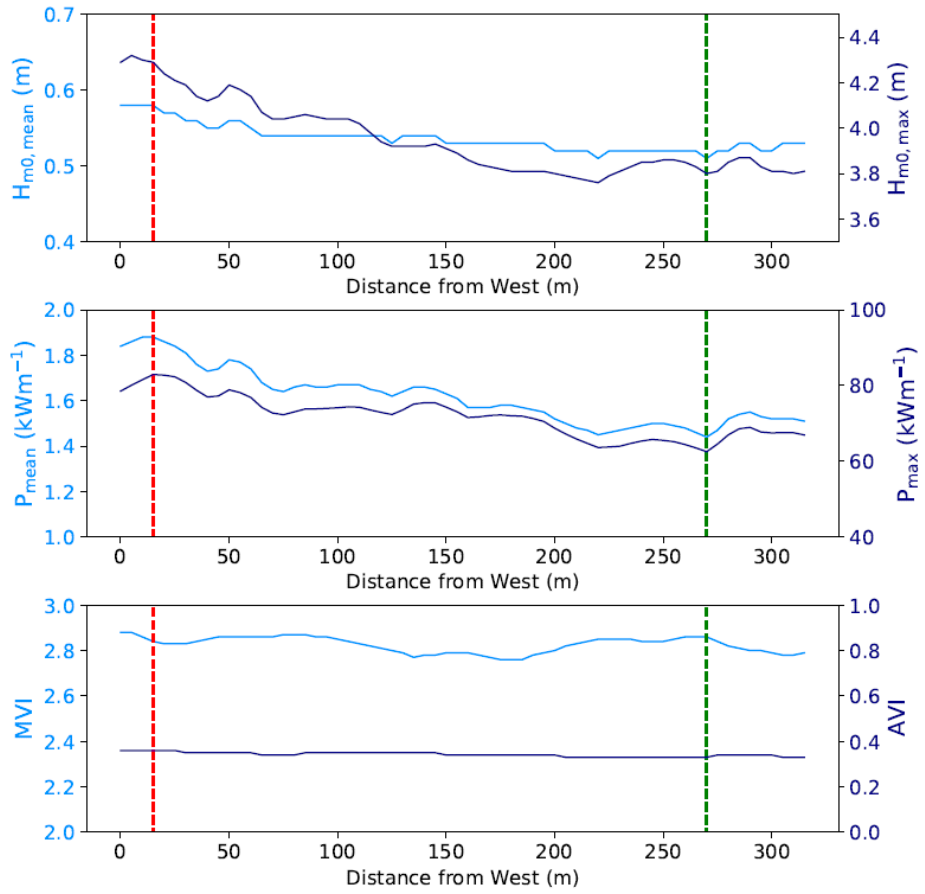

Figure 7. Spatial distribution of (**top**) the averaged and maximum significant wave heights, (**center**) the averaged and maximum available wave energy fluxes and (**bottom**) the monthly and annual variability indexes (MVI and AVI) computed from SWAN predictions along the line considered offshore from the harbour breakwater. The vertical dotted red and green lines show the locations of points considered for the investigation of WEC performance in Section 4.3. Please also note that different vertical axes are used for these parameters.

The temporal variability of the available wave energy flux was investigated by spatially averaging along the line off the harbour breakwater. Figure 8 shows the monthly variations obtained during the ten-year period from 2006 to 2015. These time series exhibited interseasonal and interannual variability of the wave resource, quite typical for this marine renewable energy over the northwest European shelf seas [41,42]. Important interannual variability was therefore exhibited during the winter period. Thus, for the month of March, we obtained mean wave powers of 4.40 kW m^{-1} in 2008 against 1.15 kW m^{-1} in 2012. This monthly variability remained important for the different extraction points considered off the harbour breakwater, with values of monthly variability indexes (MVI) over 2.75 (Figure 7). Such values were comparable to indexes obtained in energetic locations, including the northern oceanic region off the USA East Coast [44]. However, the available wave power showed more steady values at the annual scales with reduced annual variability indexes (AVI) below 0.50. Thus, over the ten-year period considered, the yearly averaged available wave power was characterised by differences below 0.7 kW m^{-1} (Figure 9). In the area considered off the harbour breakwater, the wave energy resource was therefore characterised by increased seasonal and monthly variability but appeared to show more restricted differences at the annual scale.

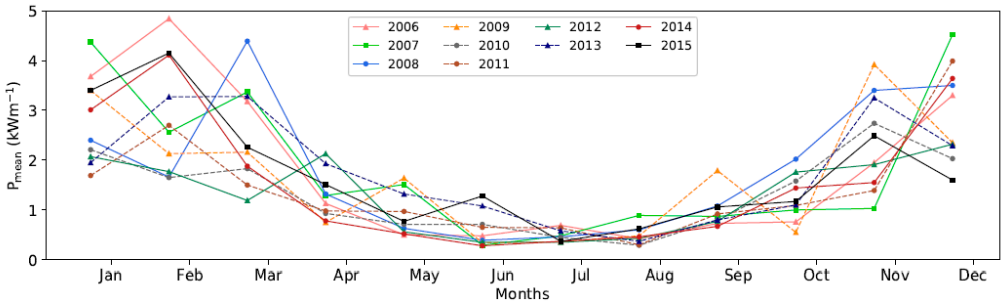

Figure 8. Yearly time series of the monthly variations of predicted available wave power averaged along the line offshore from the harbour breakwater.

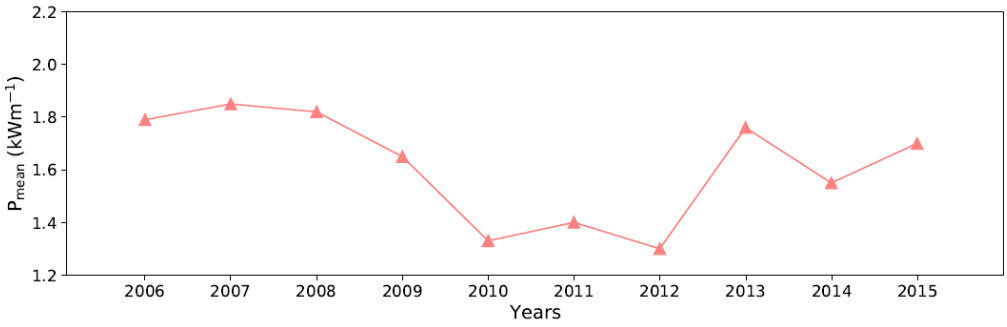

Figure 9. Time series of the yearly available wave power averaged along the line offshore from the harbour breakwater.

4.3. Annual and Seasonal Variability of Onshore WEC Performance

Estimating the energy output from WEC depends naturally on the technological characteristics and performance of the devices. Thus, for a great number of resource assessments, the expected technical power was evaluated by coupling wave numerical predictions with device power matrices, which provided the distribution of expected energy output for different classes of significant wave heights and wave periods (see [8] for a review). However, given the diversity of WEC technologies and designs, it appeared very difficult to conduct an extended investigation of energy exploitation off the harbour breakwater. For these reasons, we relied instead on the generic approach proposed by Portilla et al. [45], who evaluated WEC performance as a function of operating scenarios (for energy exploitation) based on the installed capacity. This approach, independent from the device technology, was complemented by a refined evaluation that tested the performance of a series of scaled prototypes off the harbour breakwater.

4.3.1. Generic Assessment

Following the approach proposed by Portilla et al. [45], we assumed that the available wave energy flux was directly converted into energy output depending on the installed capacity of the devices. Such an approach neglected the variations of energy output for different combinations of wave heights and periods as integrated with the power matrix. Indeed, with the approach based on the power matrix, for a given H_{m0}, the device generates energy as a function of the wave period, which may result in a highly variable production depending on the sea state (swell, local wind-generated waves, etc.). However, the approach proposed by Portilla et al. [45] allows an energy assessment independent from the device technology before conducting refined investigations based on power matrices (described in Section 4.3.2). In this approach, the installed capacity IC was expressed as the energy flux in W m^{-1}. It refers to the amount of energy that would be produced by WEC operating at its full capacity. With these assumptions, for a given IC, we evaluated

the amount of energy that would be produced at different time steps depending on the available wave energy flux. To match realistic conditions, we furthermore considered three operating modes: (i) a first mode with low energetic conditions not sufficient to trigger energy exploitation with respect to WEC performance, (ii) a second mode with the device starting to convert the available wave energy flux under the upper limit of IC and (iii) a third mode with WEC halting to guarantee the protection of the structure and enter into survival mode. According to [44,45], the lower and upper limits were fixed to 20% and 120% of the installed capacity. Following this method, the annual energy production, AEP, was computed as the total energy produced by WEC during a year, and was therefore expressed in Whm^{-1} $year^{-1}$. The capacity factor, CF, was finally determined as the ratio between the annual energy production and the total energy produced by a device operating at its full IC. Thus, CF was expressed in percentages exhibiting WEC performance and therefore providing insights about the relevance of investments.

Following the assessment of the available wave energy resource described in Section 4.2, the method was applied at the western and eastern ends of the line considered off the infrastructure, these two locations exhibiting contrasting wave exposure (Figure 7). Confirming results obtained by Portilla et al. [45], the evolution of AEP and CF exhibited, in both cases, peak values with respect to the installed capacity (Figure 10). Indeed, the annual production showed a peak value when WEC captured the maximum available wave power between the lower and upper limits of 20–120% the IC. Thus, WEC with reduced IC only captured the lower part of the available wave energy flux whereas WEC with high IC failed to operate at full capacity, thus restricting the production to storm conditions. In other words, for lowest IC, energy output resulted from the upper limit of 120% IC, whereas, for highest IC, energy output derived from the lower limit of 20% IC. Furthermore, peaks for AEP and CF were obtained for different values of IC exhibiting that high WEC performance tended to be reached for low IC. We obtained improved performance and stronger annual production at the western location than at the eastern point in relation to more wave energetic conditions. However, at both locations AEP was characterised by low values below 10 $MWhm^{-1}$ $year^{-1}$ that contrasted with values over 100 $MWhm^{-1}$ $year^{-1}$ obtained in offshore waters of the North Atlantic Ocean [44,45]. Nevertheless, CF showed improved performance of WEC for reduced IC with averaged values liable to exceed 20%.

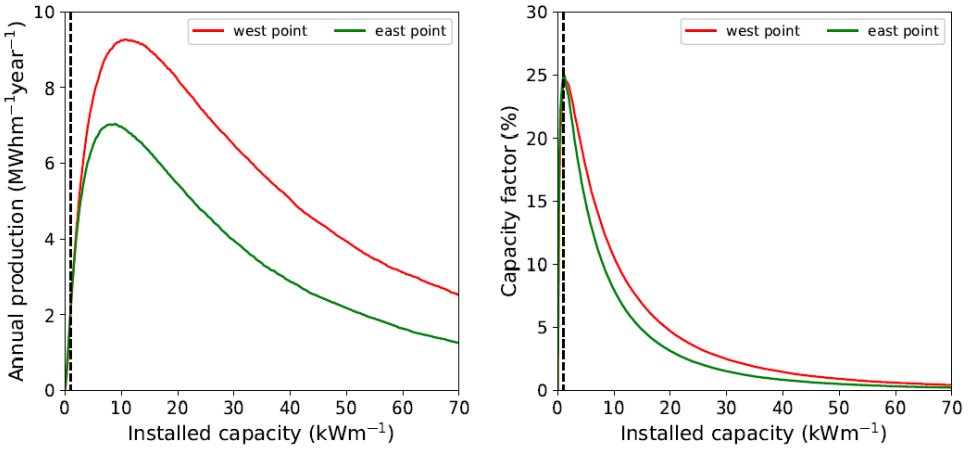

Figure 10. Predicted mean (**left**) annual energy production and (**right**) capacity factor against the installed capacity at the two locations considered at the western and eastern ends of the line offshore from the harbour breakwater and during the ten-year period from 2006 to 2015. The vertical black line shows the position of peak capacity factor reached for an installed capacity around 1.0/1.25 kW m^{-1}.

Thus, the installed capacity has to be adapted to local wave conditions to guarantee a balance between energy output and WEC performance. In the present investigation, the results obtained showed that the vicinity of the breakwater was adapted to devices with reduced IC. This corresponds typically to small-scale WECs implemented in the marine

environment, such as prototypes, to test performances in actual sea conditions before targeting more energetic locations.

4.3.2. Assessment Based on Small-Scale Prototypes

Refined investigation of WEC performance in this environment requires access to power matrices of devices that characterise the energy output over a range of significant wave heights and wave periods. However, whereas a part of these power matrices are available from WEC developers, the associated distribution is associated to a technology designed to specific wave conditions, typically the energetic wave climate of targeted sites. Thus, power matrices adapted to "hot spots" with strong wave conditions cannot be exploited off the harbour breakwater with conditions more suitable to the implementation of small-scaled prototypes (Section 4.3.1). The evaluation of WEC performance off Roscoff breakwater therefore required the exploitation of power matrices of scaled devices with different ratings.

These power matrices were obtained by applying the method described by Payne [46] and applied in a series of investigations dealing with the scaling of WEC to local sea states [47–51] Thus, following this approach, the original power matrix of a given technology was scaled for different sizes of devices by assuming that the Froude number remained constant between small-scaled prototypes. Thus, according to Froude scaling law, wave heights were scaled linearly with the geometric scale λ, wave periods with the square root of λ and power as $\lambda^{3.5}$. Further details about the theoretical description and assumptions of this method, and its practical implementation, are available in [46,47]. O'Connor et al. [47] relied on this approach to assess the performance of Wave Star and Pelamis at various scales in different locations within the European shelf seas. Bozzi et al. [48,51] applied the method (i) to AquaBuOY, Pelamis and Wave Dragon at two energetic locations around Italy and (ii) to eight wave energy technologies along the Mediterranean coastline. Majidi Nezhad et al. [50] exploited this method to evaluate the performance of four technologies, including Wave Star, Oyster, Wave Dragon and Archimedes Wave Swing, on the west coast of Sicily (Italy). More recently, Majidi et al. [49] evaluated the performance of 15 WECs in different water depths along the southwestern coast of the Black Sea.

As a preliminary assessment of small-scale WEC performance, the present investigation was restricted to one technology, the oscillating flap Oyster [18,19]. Compared to other devices designed to be implemented in offshore waters, the Oyster may operate nearshore within around 10–15 m water depth, thus matching environmental conditions off the harbour breakwater. Furthermore, this device was considered to provide better performance than the heaving buoy [52,53]. The power matrix considered as the initial reference to be scaled has a rated power of 290 kW [54,55]. For this power matrix, optimal performances were reached for significant wave heights between 4 and 6 m and wave energy periods between 7 and 10 s. This was clearly out of the scope of the mean distribution of wave events off the harbour breakwater (Figure 11), thus promoting the exploitation of scaled power matrices with scaled wave heights and wave periods adapted to the local wave climate.

Following the generic assessment of WEC performances described in Section 4.3.1, the method was applied to the location considered at the western end of the line off the harbour breakwater. Furthermore, scaled power matrices were established taking into account of constraints applied on the mechanical parts of devices. Thus, to be consistent with WEC designs, energy output was only considered over the range of scaled wave heights and wave periods.

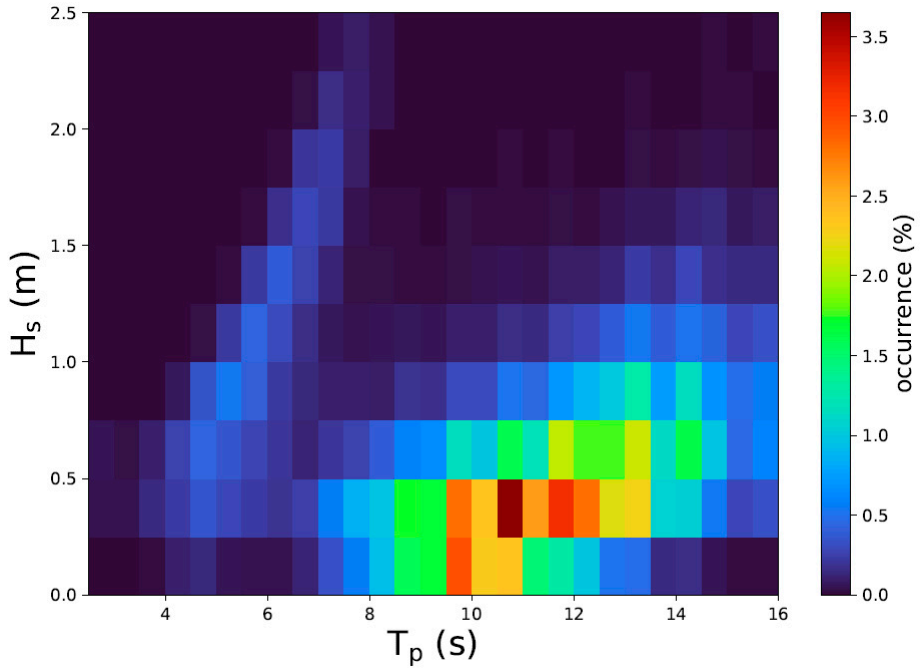

Figure 11. Mean distribution of wave events for a range of significant wave heights H_s and peak periods T_p, at the western end of the line offshore from the harbour breakwater during the ten-year period from 2006 to 2015. The color bar shows the occurrence of waves events in percentages.

Figure 12 shows the resulting evolution of the capacity factor and the annual energy production as a function of the rated power for the different scaled prototypes of the Oyster device. The capacity factor CF was found to decrease with the rated power whereas the production appeared to increase. Following the generic assessment described in Section 4.3.1 (Figure 10), the rated power considered remained, therefore, (i) over the peak of maximum capacity factor (which was very low for the site of application) and (ii) below the peak of annual production with respect to the installed capacity. We also obtained reduced values of CF for the different rated powers in comparison with the generic assessment. Thus, the capacity factor of the Oyster devices remained below 12% whereas it exceeded 20% in the generic assessment. Indeed, the previous generic estimation considered that wave energy flux was directly converted into energy output, whereas only a part of the available resource was exploited by scaled devices, depending on the significant wave height and the wave period. However, this second evaluation appeared more realistic, providing a refined assessment of the expected performance of small-scale devices off the harbour breakwater. Thus, maximum performances, with capacity factors over 8%, were obtained for devices with low ratings below 90 kW. These averaged values were less important than values expected for WEC in offshore waters [54,56]. However, as the available resource, the capacity factor also exhibited important temporal variations liable to reach values over 20% during the winter period as exhibited by the monthly evolution of CF for a scaled Oyster WEC with a nominal power of 90 kW (Figure 13). Thus, whereas the vicinity of the harbour showed restricted interest for an extended exploitation of the wave energy resource, it may be considered as an experimental site for testing small-scale prototypes of wave energy converters in western Brittany, having the advantages of (i) a wide panel of sea wave conditions (including swell and wind seas) and (ii) reduced effects of the tide on WEC operation (which may be significant in western Brittany, characterised by important wetting–drying areas along the coastline). Therefore, results provided further insights concerning the expected performance of these small-scale prototypes in this environment.

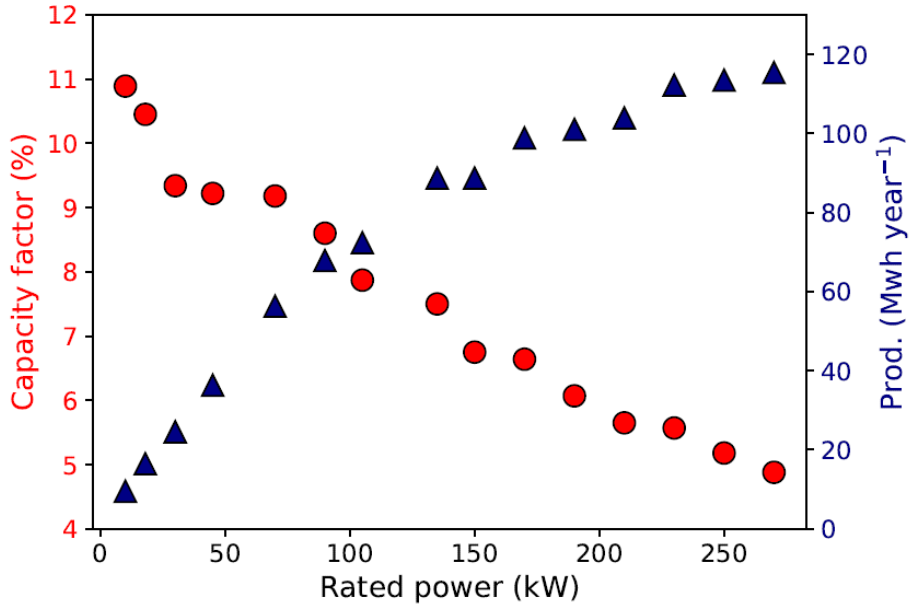

Figure 12. Capacity factor and mean annual production as a function of the rated power of scaled Oyster prototypes at the western end of the line offshore from the harbour breakwater over the ten-year period from 2006 to 2015.

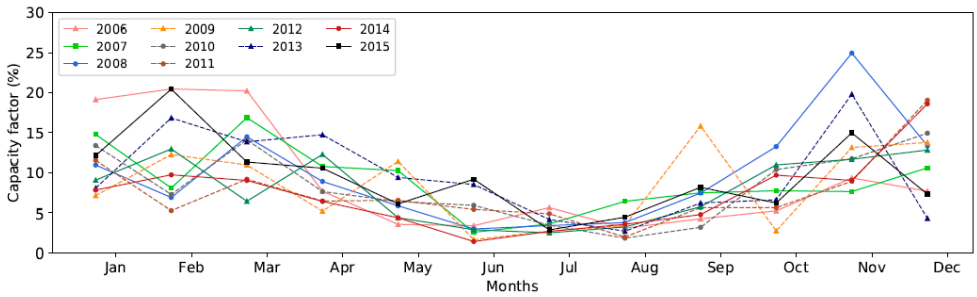

Figure 13. Yearly time series of the monthly variations of predicted capacity factor from a Oyster prototype with a rated power of 90 kW at the western end of the line offshore from the harbour breakwater over the ten-year period from 2006 to 2015.

5. Conclusions

A refined assessment of the available wave energy resource and technically exploitable energy output was conducted in the vicinity of the harbour of Roscoff breakwater (northern Brittany, France). This evaluation relied on (i) a hindcast database of the wave climate derived from numerical simulations conducted at high spatial resolution near the harbour infrastructure, (ii) a generic assessment of WEC performance and (iii) a refined evaluation based on a series of scaled power matrices associated with the Oyster technology. The main outcomes of the present investigation follow:

1. The phase-averaged spectral wave model SWAN reproduced the observed evolution of wave conditions in offshore and nearshore waters, including the vicinity of the harbour breakwater. Thus, besides approaching the observed variations between storm and calm weather conditions, the model reproduced the semidiurnal modulations of significant wave heights and incoming wave directions resulting from tide-induced refraction.
2. In order to gain further insights about the spatiotemporal variability of the wave energy flux in the vicinity of the harbour, these predictions were exploited to produce a hindcast database of the available resource, over the ten-year period from 2006 to

2015, along a line offset at a distance of 100 m from the breakwater. The surroundings of the harbour showed a spatial gradient in the distribution of significant wave height and energy flux, associated with increased exposure of the northwestern area off the rockfill section at the foot of the breakwater.

3. Along this line, the available resource was characterised by increased seasonal and monthly variability, exhibiting prominent differences between the winter and the summer periods. It showed, however, more restricted differences at the annual scales.
4. The generic assessment of WEC energy production showed increased performance for a low capacity installation, exhibiting the interest of the site of application for the implementation of small-scale devices. Thus, the refined evaluation based on scaled power matrices derived from the Oyster technology confirmed this first assessment. Furthermore, the capacity factor was characterised by increased seasonal variability reaching values over 20% during the winter period.

These results therefore promote the interest of the harbour of Roscoff as an experimental site for testing the performance of small-scale WECs, off the breakwater, with (i) a wide range of wave conditions (including swell and wind seas), (ii) reduced effects of tidal range on devices operation and (iii) wave constraints adapted to the design of mechanical structures. Furthermore, this local application exhibits the progress reached in resource assessment by combining (i) a refined evaluation of wave conditions with (ii) a detailed evaluation of WEC power matrices. We propose here an original investigation dedicated to the performance of small-scale devices on a moderate-energy site. However, this method may also be applied to more energetic locations dominated by ocean swell (and more adapted to a large-scale exploitation of the resource) where we also expect improved performance of the phase-averaged spectral wave model. Indeed, for these different applications, the wave energy converter has to be adapted to the local wave climate. Thus, the installed capacity and rated power of energy converters are established to guarantee the balance between a minimum amount of energy output and high WEC performance. This aspect is fundamental for the development of a device as increasing the installed capacity requires significant capital investments liable to reduce the economical yield and profitability of the targeted technology. The method proposed may help to refine these estimations in the preliminary stages of a wave energy project. In energetic locations, such an approach should finally be complemented by a refined evaluation of economic performance of devices for the different designs and ratings. Thus, the optimised rating power will also be established by analysing the economic cost of a wave energy project with indicators such as the levelised cost of energy, which integrates production and costs associated with capital expenditure, together with operation and maintenance. Further studies may be conducted on the performance of WECs attached to the quay side, where wave reflection effects have to be considered and may improve the performance of energy converters.

Author Contributions: N.G.: conceptualization, methodology, software, validation, formal analysis, investigation, writing—original draft, writing—review and editing, visualization, supervision, and project administration. G.C.: writing—review and editing, and project administration. P.S.: writing—review and editing, and project administration. All authors have read and agreed to the published version of the manuscript.

Funding: A part of this study was conducted for the Region Brittany (France) to identify potential locations in harbour areas for the implementation of wave energy converters.

Institutional Review Board Statement: Not applicable.

Informed Consent Statement: Not applicable.

Data Availability Statement: Not applicable.

Acknowledgments: The present paper is a contribution to the research program of the team "Hydraulique et Aménagement" (Cerema, DTecREM, http://www.cerema.fr (accessed on 23 June 2022)). The authors warmly thank the harbour authorities of Roscoff–Bloscon for the discussion and exchanges about the exploitation and design of the breakwater "Pierre Lemaire". Numerical simulations and treatments of hindcast databases were conducted on computer facilities DATARMOR of "Pôle de Calcul et de Données pour la Mer" (PCDM) (https://wwz.ifremer.fr/pcdm, accessed on 23 June 2022).

Conflicts of Interest: The authors declare no conflict of interest.

References

1. Cascajo, R.; García, E.; Quiles, E.; Correcher, A.; Morant, F. Integration of Marine Wave Energy Converters into Seaports: A Case Study in the Port of Valencia. *Energies* **2019**, *12*, 787. [CrossRef]
2. Sergent, P.; Baudry, V.; De Bonviller, A.; Michard, B.; Dugor, J. Numerical Assessment of Onshore Wave Energy in France: Wave Energy, Conversion and Cost. *J. Mar. Sci. Eng.* **2020**, *8*, 947. [CrossRef]
3. Ingine Inc.—Harness Nature Power. Available online: https://ingine.co.kr/en/ (accessed on 15 June 2022).
4. Eco Wave Power—Wave Energy Company. Available online: http://www.ecowavepower.com (accessed on 15 June 2022).
5. Contestabile, P.; Di Lauro, E.; Buccino, M.; Vicinanza, D. Economic Assessment of Overtopping BReakwater for Energy Conversion (OBREC): A Case Study in Western Australia. *Sustainability* **2016**, *9*, 51. [CrossRef]
6. Contestabile, P.; Ferrante, V.; Di Lauro, E.; Vicinanza, D. Prototype Overtopping Breakwater for Wave Energy Conversion at Port of Naples. In Proceedings of the 26th International Ocean and Polar Engineering Conference, Rhodes, Greece, 26 June 2016; p. ISOPE-I-16-418.
7. Arena, F.; Romolo, A.; Malara, G.; Fiamma, V.; Laface, V. The First Full Operative U-OWC Plants in the Port of Civitavecchia. In *Proceedings of the Volume 10: Ocean Renewable Energy*; American Society of Mechanical Engineers: Trondheim, Norway, 2017.
8. Ibarra-Berastegi, G.; Ulazia, A.; Sáenz, J.; Serras, P.; González Rojí, S.J.; Esnaola, G.; Iglesias, G. The Power Flow and the Wave Energy Flux at an Operational Wave Farm: Findings from Mutriku, Bay of Biscay. *Ocean. Eng.* **2021**, *227*, 108654. [CrossRef]
9. Guillou, N.; Lavidas, G.; Chapalain, G. Wave Energy Resource Assessment for Exploitation—A Review. *J. Mar. Sci. Eng.* **2020**, *8*, 705. [CrossRef]
10. IEC. *Marine Energy—Wave, Tidal and Other Water Current Converters—Part 101: Wave Energy Resource Assessment and Characterization*; International Electrotechnical Commission/Technical Specification: Geneva, Switzerland, 2014.
11. ISO. *Petroleum and Natural Gas Industries—Specific Requirements for Offshore Structures—Part 1: Metocean Design and Operating Considerations*; The International Organization for Standardization: Geneva, Switzerland, 2015.
12. IMAREST. *Metocean Procedures Guide for Offshore Renewables*; Institute of Marine Engineering, Science & Technology (Offshore Renewables Special Interest Group): London, UK, 2018.
13. Reguero, B.G.; Losada, I.J.; Méndez, F.J. A Recent Increase in Global Wave Power as a Consequence of Oceanic Warming. *Nat. Commun.* **2019**, *10*, 205. [CrossRef] [PubMed]
14. Penalba, M.; Aizpurua, J.I.; Martinez-Perurena, A.; Iglesias, G. A Data-Driven Long-Term Metocean Data Forecasting Approach for the Design of Marine Renewable Energy Systems. *Renew. Sustain. Energy Rev.* **2022**, *167*, 112751. [CrossRef]
15. Lastiri, X.; Abadie, S.; Maron, P.; Delpey, M.; Liria, P.; Mader, J.; Roeber, V. Wave Energy Assessment in the South Aquitaine Nearshore Zone from a 44-Year Hindcast. *JMSE* **2020**, *8*, 199. [CrossRef]
16. Booij, N.; Ris, R.C.; Holthuijsen, L.H. A Third-Generation Wave Model for Coastal Regions: 1. Model Description and Validation. *J. Geophys. Res. Ocean.* **1999**, *104*, 7649–7666. [CrossRef]
17. Cascajo, R.; García, E.; Quiles, E.; Morant, F.; Correcher, A. Wave Energy Assessment at Valencia Gulf and Comparison of Energy Production of Most Suitable Wave Energy Converters. *IJERPH* **2020**, *17*, 8473. [CrossRef]
18. Cameron, L.; Doherty, K.; Doherty, R.; Henry, A.; Van't Hoff, J.; Kaye, D.; Naylor, D.; Bourdier, S.; Whittaker, T. Design of the Next Generation of the Oyster Wave Energy Converter. In Proceedings of the 3rd International Conference on Ocean Energy, Bilbao, Spain, 6–9 October 2010.
19. O'Boyle, L.; Doherty, K.; Hoff, J.V.; Skelton, J. The Value of Full Scale Prototype Data—Testing Oyster 800 at EMEC, Orkney. In Proceedings of the 11th European Wave and Tidal Energy Conference (EWTEC), Nantes, France, 6–11 September 2015.
20. SHOM. 2022. Available online: https://www.data.shom.fr (accessed on 5 July 2022).
21. Holthuijsen, L.H. *Waves in Oceanic and Coastal Waters*, 1st ed.; Cambridge University Press: Cambridge, UK, 2007; ISBN 978-0-521-86028-4.
22. Guillou, N. Modelling Effects of Tidal Currents on Waves at a Tidal Stream Energy Site. *Renew. Energy* **2017**, *114*, 180–190. [CrossRef]
23. Komen, G.J.; Cavaleri, L.; Donelan, M.; Hasselmann, K.; Hasselmann, S.; Janssen, P.A.E.M. *Dynamics and Modelling of Ocean Waves*, 1st ed.; Cambridge University Press: Cambridge, UK, 1994; ISBN 978-0-521-57781-6.

24. Rogers, W.E.; Babanin, A.V.; Wang, D.W. Observation-Consistent Input and Whitecapping Dissipation in a Model for Wind-Generated Surface Waves: Description and Simple Calculations. *J. Atmos. Ocean. Technol.* **2012**, *29*, 1329–1346. [CrossRef]
25. Hasselmann, S.; Hasselmann, K.; Allender, J.H.; Barnett, T.P. Computations and Parameterizations of the Nonlinear Energy Transfer in a Gravity-Wave Specturm. Part II: Parameterizations of the Nonlinear Energy Transfer for Application in Wave Models. *J. Phys. Oceanogr.* **1985**, *15*, 1378–1391. [CrossRef]
26. Bouws, E.; Komen, G.J. On the Balance Between Growth and Dissipation in an Extreme Depth-Limited Wind-Sea in the Southern North Sea. *J. Phys. Oceanogr.* **1983**, *13*, 1653–1658. [CrossRef]
27. Eldeberky, Y.; Battjes, J.A. Spectral Modeling of Wave Breaking: Application to Boussinesq Equations. *J. Geophys. Res. Ocean.* **1996**, *101*, 1253–1264. [CrossRef]
28. Battjes, J.A.; Janssen, J.P.F.M. Energy Loss and Set-up Due to Breaking Random Waves. In Proceedings of the 16th Conference on Coastal Engineering, Hamburg, Germany, 27 August–3 September 1978.
29. The SWAN Team. *SWAN—Scientific and Technical Documentation*; Delft University of Technology: Delft, The Netherlands, 2017.
30. SHOM. *MNT Bathymétrique de façade Atlantique (Projet HOMONIM)*; Technical Report; 2015. [CrossRef]
31. SHOM. *Litto3D—Version 1.0—Descriptif Du Contenu*; Technical Report; 2015; p. 32.
32. Pierson, W.J., Jr.; Moskowitz, L. A Proposed Spectral Form for Fully Developed Wind Seas Based on the Similarity Theory of S. A. Kitaigorodskii. *J. Geophys. Res.* **1964**, *69*, 5181–5190. [CrossRef]
33. Boudière, E.; Maisondieu, C.; Ardhuin, F.; Accensi, M.; Pineau-Guillou, L.; Lepesqueur, J. A Suitable Metocean Hindcast Database for the Design of Marine Energy Converters. *Int. J. Mar. Energy* **2013**, *3–4*, e40–e52. [CrossRef]
34. MARC—Modélisation et Analyse Pour La Recherche Cotière. Available online: https://marc.ifremer.fr/ (accessed on 15 June 2022).
35. Hanna, S.R.; Heinold, D. *Development and Application of a Simple Method for Evaluating Air Quality*; American Petroleum Institute: Washington, DC, USA; Health and Environmental Affairs Department: Washington, DC, USA, 1985.
36. Kalourazi, M.Y.; Siadatmousavi, S.M.; Yeganeh-Bakhtiary, A.; Jose, F. WAVEWATCH-III Source Terms Evaluation for Optimizing Hurricane Wave Modeling: A Case Study of Hurricane Ivan. *Oceanologia* **2021**, *63*, 194–213. [CrossRef]
37. Mentaschi, L.; Besio, G.; Cassola, F.; Mazzino, A. Problems in RMSE-Based Wave Model Validations. *Ocean. Model.* **2013**, *72*, 53–58. [CrossRef]
38. Cornett, A. A Global Wave Energy Resource Assessment. In Proceedings of the International Offshore and Polar Engineering Conference, Vancouver, BC, Canada, 6 July 2008.
39. Gonçalves, M.; Martinho, P.; Guedes Soares, C. A 33-Year Hindcast on Wave Energy Assessment in the Western French Coast. *Energy* **2018**, *165*, 790–801. [CrossRef]
40. Guillou, N. Evaluation of Wave Energy Potential in the Sea of Iroise with Two Spectral Models. *Ocean. Eng.* **2015**, *106*, 141–151. [CrossRef]
41. Guillou, N.; Chapalain, G. Numerical Modelling of Nearshore Wave Energy Resource in the Sea of Iroise. *Renew. Energy* **2015**, *83*, 942–953. [CrossRef]
42. Neill, S.P.; Hashemi, M.R. Wave Power Variability over the Northwest European Shelf Seas. *Appl. Energy* **2013**, *106*, 31–46. [CrossRef]
43. Mentaschi, L.; Besio, G.; Cassola, F.; Mazzino, A. Performance Evaluation of Wavewatch III in the Mediterranean Sea. *Ocean. Model.* **2015**, *90*, 82–94. [CrossRef]
44. Guillou, N.; Chapalain, G. Assessment of Wave Power Variability and Exploitation with a Long-Term Hindcast Database. *Renew. Energy* **2020**, *154*, 1272–1282. [CrossRef]
45. Portilla, J.; Sosa, J.; Cavaleri, L. Wave Energy Resources: Wave Climate and Exploitation. *Renew. Energy* **2013**, *57*, 594–605. [CrossRef]
46. Payne, G. Guidance for the Experimental Tank Testing of Wave Energy Converters. *Supergen Mar.* **2008**, *254*, 1–51.
47. O'Connor, M.; Lewis, T.; Dalton, G. Techno-Economic Performance of the Pelamis P1 and Wavestar at Different Ratings and Various Locations in Europe. *Renew. Energy* **2013**, *50*, 889–900. [CrossRef]
48. Bozzi, S.; Archetti, R.; Passoni, G. Wave Electricity Production in Italian Offshore: A Preliminary Investigation. *Renew. Energy* **2014**, *62*, 407–416. [CrossRef]
49. Majidi, A.; Bingölbali, B.; Akpınar, A.; Iglesias, G.; Jafali, H. Downscaling Wave Energy Converters for Optimum Performance in Low-Energy Seas. *Renew. Energy* **2021**, *168*, 705–722. [CrossRef]
50. Majidi Nezhad, M.; Groppi, D.; Rosa, F.; Piras, G.; Cumo, F.; Garcia, D.A. Nearshore Wave Energy Converters Comparison and Mediterranean Small Island Grid Integration. *Sustain. Energy Technol. Assess.* **2018**, *30*, 68–76. [CrossRef]
51. Bozzi, S.; Besio, G.; Passoni, G. Wave Power Technologies for the Mediterranean Offshore: Scaling and Performance Analysis. *Coast. Eng.* **2018**, *136*, 130–146. [CrossRef]
52. Babarit, A.; Hals, J.; Muliawan, M.J.; Kurniawan, A.; Moan, T.; Krokstad, J. Numerical Benchmarking Study of a Selection of Wave Energy Converters. *Renew. Energy* **2012**, *41*, 44–63. [CrossRef]
53. Baudry, V.; Marrone, S.; Babarit, A.; Le Touzé, D.; Clément, A.H. Power Matrix Assessment and Extreme Loads Estimation on a Flap Type Wave Energy Converter in Front of a Dike. In Proceedings of the EWTEC, Nantes, France, 6–11 September 2015.

54. Carballo, R.; Sánchez, M.; Ramos, V.; Fraguela, J.A.; Iglesias, G. The Intra-Annual Variability in the Performance of Wave Energy Converters: A Comparative Study in N Galicia (Spain). *Energy* **2015**, *82*, 138–146. [CrossRef]
55. Silva, D.; Rusu, E.; Soares, C. Evaluation of Various Technologies for Wave Energy Conversion in the Portuguese Nearshore. *Energies* **2013**, *6*, 1344–1364. [CrossRef]
56. Guillou, N.; Chapalain, G. Annual and Seasonal Variabilities in the Performances of Wave Energy Converters. *Energy* **2018**, *165*, 812–823. [CrossRef]